The Three-Dimensional Micro- and Nanostructure of the Aortic Medial Lamellar Unit Measured Using 3D Confocal & Electron Microscopy Imaging

Mary K O'Connell[a], **Sushila Murthy**[a], **Samson Phan**[b], **Chengpei Xu**[c], **JoAnn Buchanan**[d], **Ryan Spilker**[a], **Ronald L Dalman**[c], **Christopher K Zarins**[c], **Winfried Denk**[e], and **Charles A Taylor**[b,c]

[a]*Department of Mechanical Engineering, Stanford University, Stanford, CA*

[b]*Department of Bioengineering, Stanford University, Stanford, CA*

[c]*Department of Surgery, Stanford University, Stanford, CA*

[d]*Department of Molecular and Cellular Physiology, Stanford University, Stanford, CA*

[e]*Max-Planck Institute for Medical Research, Heidelberg, Germany*

Abstract

Changes in arterial wall composition and function underlie all forms of vascular disease. The fundamental structural and functional unit of the aortic wall is the medial lamellar unit (MLU). While the basic composition and organization of the MLU is known, three-dimensional (3D) microstructural details are tenuous, due (in part) to lack of three-dimensional data at micro- and nano-scales. We applied novel electron and confocal microscopy techniques to obtain 3D volumetric information of aortic medial microstructure at micro- and nano-scales with all constituents present. For the rat abdominal aorta, we show that medial elastin has three primary forms: with approximately 71% of total elastin as thick, continuous lamellar sheets, 27% as thin, protruding interlamellar elastin fibers (IEFs), and 2% as thick radial struts. Elastin pores are not simply holes in lamellar sheets, but are indented and gusseted openings in lamellae. Smooth Muscle Cells (SMCs) weave throughout the interlamellar elastin framework, with cytoplasmic extensions abutting IEFs, resulting in approximately 20° radial tilt (relative to the lumen surface) of elliptical SMC nuclei. Collagen fibers are organized as large, parallel bundles tightly enveloping SMC nuclei. Quantification of the orientation of collagen bundles, SMC nuclei, and IEFs reveal that all three primary medial constituents have predominantly circumferential orientation, correlating with reported circumferentially dominant values of physiological stress, collagen fiber recruitment, and tissue stiffness. This high resolution three-dimensional view of the aortic media reveals MLU microstructure details that suggest a highly complex and integrated mural organization that correlates with aortic mechanical properties.

Corresponding Author: Charles A. Taylor Clark Center, Room E350B 318 Campus Drive Stanford, CA 94305 (650) 725-6128 (650) 725-9082 Fax E-mail: taylorca@stanford.edu. Reprint Requests: Send to corresponding author.

Keywords

Extracellular matrix; microstructure; elastin; medial lamellar unit; smooth muscle cells; collagen; aorta

Introduction

The medial lamellar unit (MLU) is both the structural and functional unit of the aorta, observed in the aorta of all mammals (Wolinsky and Glagov, 1967). MLU layers are repeated throughout the thickness of the wall, with MLU quantity proportional to the circumferential tension in the arterial wall (Wolinsky and Glagov, 1967). Aortic elastic properties are similar for differently sized animals (Dobrin, 1983) and tension per MLU remains essentially constant at approximately 2 N/m (Wolinsky and Glagov, 1964; Zatina et al., 1984). Additionally, orientation of extracellular matrix (ECM) fibers within the MLU affects the distribution of stresses and vice-versa (Clark and Glagov, 1985; Driessen et al., 2003; Gosline and Shadwick, 1996; Jackson et al., 2002; Kanda and Matsuda, 1994; Loree et al., 1992; Sun et al., 2004). MLU structure is related to function.

Wolinsky and Glagov proposed the first model of MLU microstructure in 1967, describing the MLU as concentric elastic lamellae with smooth muscle cells (SMCs) and collagen in between (Wolinsky and Glagov, 1967). Numerous subsequent studies of blood vessel microstructure have enhanced this model, but the lack of high resolution three-dimensional (3D) data has resulted in unclear and often contradictory descriptions of mural microstructure.

In Clark and Glagov's MLU model, interlamellar space was filled with overlapping SMCs, thin, circumferentially oriented elastin fibrils, and wavy collagen fibers. SMCs are depicted as elongated nuclei surrounded by smooth cytoplasm spanning between lamellae, with wavy collagen and interlamellar elastin fibers (IEFs) weaving throughout. The number of lamellae has been shown to decrease from anterior to posterior (Draney, 2003) and from superior to inferior, and branching of one lamella into two distinct lamellae has been observed (Berry CL, 1972; Gerrity, 1972; Smith, 1976). Direct connections between lamellae have been observed in 2D images and chemically degraded specimens (Berry CL, 1972; Smith, 1976; Song SH, 1985), and more recent studies described considerable interlamellar elastin (Dingemans et al., 2000; Jiang CF, 1992), as well as a direct connection between elastin and SMCs (Dingemans et al., 2000).

Many SMC features are controversial. SMC orientation is described as circumferential (Arner and Uvelius, 1982; Clark and Glagov, 1985; Dingemans et al., 2000; Gaballa et al., 1998; Hansen et al., 1980; Wolinsky and Glagov, 1967), oblique (Bierring and Kobayasi, 1963; Cliff, 1967; Fujiwara and Uehara, 1992; Keech, 1960; Wolinsky and Glagov, 1967), and helical (Gabella, 1983; Osborne-Pellegrin, 1978; Wolinsky and Glagov, 1967). SMC orientation relative to the vessel surface has been described as parallel (Clark and Glagov, 1985) and not parallel (Cliff, 1970; Fujiwara and Uehara, 1992; Keech, 1960; Pease and Paule, 1960). Both SMC and IEF orientation has been observed to change directions in each subsequent lamella, creating a herringbone appearance when viewed in longitudinal section (Davis, 1993; Dingemans et al., 2000). In addition, collagen fibers are described as wrapping around the vessel in a helical organization (Rhodin, 1979; Shadwick, 1999; Walker-Caprioglio et al., 1991; Wolinsky and Glagov, 1964). Collagen takes the form of membranes enveloping SMCs and the form of wavy bundles associated closely with elastin but not with SMCs (Cliff, 1970; Dingemans et al., 2000).

Histological techniques have provided a wealth of data on mural composition. Mechanical testing has contributed information on the strength and rupture limits of aortic tissue and its individual constituents. What has been lacking in these studies is detailed information on the structural arrangement of these constituents. Previous microstructural information has come from digested specimens and 2D views. Chemical digestion is used to eliminate all material except the material of concern, so that its 3D structure can be imaged at high resolution, typically using scanning electron microscopy (SEM). However, digestion creates artifacts such as degree of degradation is difficult to control (finer features, such as thin IEFs, may be degraded while large features remain), features may be distorted (elastin pores enlarge (Song and Roach, 1984), strained material relaxes as joined components are degraded), and damage due to manipulation. Two-dimensional views are limited, and complex features can easily be misinterpreted from 2D images. A recently developed electron microscopic technique (Denk and Horstmann, 2004), produces nanostructural information in three dimensions (Briggman and Denk, 2006). The tissue is fixed in physiological conditions and imaged without removal of constituents or destruction of interconnections to create a realistic representation of the architecture and relationship of constituents. We studied the 3D MLU micro- and nanostructure of the healthy rat abdominal aorta using this technique in conjunction with confocal microscopy.

Results

The average diameter of the rat abdominal aorta shown in Figure 1 was 1.52±0.14mm, with mural thickness 118±44μm. Individual MLU thickness measured 13.9±1.2μm, and elastic lamellae measured 2.1±0.6μm thickness. Lamellae were asymmetrically numbered around the vessel circumference, with the rat abdominal aorta containing 5.3±0.5 anterior and 3.4±0.6 posterior lamellae ($p < 0.001$) (Table 1). In all specimens, lamellar quantity was greater in the anterior region compared to posterior. Elastic lamellae were observed branching in confocal laser scanning microscopy (CLSM) cross section images, with branching occurring at regular intervals around the vessel circumference (Figure 1, CLSM image shows branching). 3D CLSM (Figure 2) shows that the characteristic MLU structure, with layers of elastin divided by elongated SMC nuclei and collagen, has a highly three dimensional nature. Elastin is present between lamellae, SMC nuclei are not neatly arranged, and collagen densely fills the interlamellar space. Serial block-face scanning electron microscopy (SBFSEM) 3D volume images showed that the MLU was comprised of approximately 29% elastin, 24% SMCs, and 47% collagen and ground substance (Table 1). The 3D SBFSEM volume revealed dense packing of the MLU with elastin, SMCs, and collagen, and a complex relationship among these constituents repeated from layer to layer.

Elastin

Figure 3 shows the complex architecture of elastin having 3 unique forms: (1) Lamellae, (2) IEFs, (3) radial elastin struts. Of the 29% total elastin volume, lamellae comprised 71%. These lamellae are thick continuous sheets of elastin with a fibrous surface and periodic pores. 27% of elastin was found between lamellae, in the form of dense, intricately organized IEFs. IEFs are chords or wisps of elastin that protrude obliquely (in circumferential and radial directions) from top and bottom lamellar surfaces and terminate in interlamellar space. IEFs surrounded and abutted the SMC cytoplasm, forming a cage-like structure in which the SMC resides. The remaining 2% of elastin was found in the form of thick radial elastin struts (Table 1). Radial elastin struts, or periodic thick chords of elastin that branch from a primary elastic lamella and extend to an adjacent lamella, provided a direct radial inter-lamellar connection (Figure 3). Radial elastin struts were much less dense than IEFs, but were more substantial (90% as thick as lamellae).

The characteristic pores in elastic lamellar sheets were not merely circular perforations in lamellae, as typically represented and as observed in CLSM images (Figure 2b), but rather the high resolution of SBFSEM images showed that pores were actually indentations of lamellae whose indented edges were gusseted by extensive reinforcement from IEFs. Pores were only observed to protrude abluminally, with SMCs deforming beneath and extending into lamellar pores.

Smooth Muscle Cells

SMCs accounted for 24% of total medial volume. The volume of a single medial SMC was 1630 ± 640 μm^3, comprised of 89 ± 3% cytoplasm and 11 ± 3% nucleus. The density of SMCs within the media was $3.7\pm0.6 \times 10^5$ cells/mm^3. In 3D CLSM (Figure 2c), elongated SMC nuclei are seen layered between each set of lamellae. Figure 4 shows how the typical medial vascular SMC is configured between lamellae. The shape of healthy aortic media SMC nuclei was elliptical (long axis/ radius = 6.2 ± 1.4), averaging $3.1\pm0.8\mu m$ short axis length and $19.0 \pm3.3\mu m$ long axis length. Between lamellae, the long axis of each nucleus aligned in the circumferential direction with a $19\pm3°$ radial tilt, resulting in cytoplasmic ends directed toward top and bottom lamellae (Figure 4). This radial tilt of nuclei remained consistent from layer to layer. The cell cytoplasm had a much more irregular shape than the nucleus. The surface area-to-volume ratio of SMC cytoplasm was 18 times greater than that of its nucleus, substantiated by extensive outcroppings protruding from the main cell body encompassing the nucleus. The cytoplasm weaved in and around IEFs with extensions abutting IEF terminations and overlapping adjacent SMCs.

Collagen

Collagen and ground substance comprised 47% of the total medial volume (Table 1). 3D CLSM (Figure 2d) revealed this densely packed collagen as interspersed fibers between elastic lamellae. Higher magnification SBFSEM images showed that collagen was organized as bundles of fibers (numbering 24 ± 15 fibers per bundle), and as thin bundles or individual fibers. Figure 5 shows a series of CLSM images that reveal the parallel arrangement of collagen fiber bundles within each layer (layer refers to radial depth throughout the thickness). The orientation of each layer of parallel fiber bundles differed slightly from adjacent layers, such that a wide variety of orientations were achieved throughout the mural thickness (Figure 5). Within each layer, fiber bundles were seen closely enveloping SMC nuclei (Figure 5). Fiber bundles were coiled at mean physiological pressure (Figure 6). Individual collagen fibers were observed covering the surface of SMCs, and thin bundles were observed throughout interlamellar space.

Orientation

Figure 7 shows that all 3 primary mural constituents (IEFs, SMC nuclei, and collagen fiber bundles) aligned preferentially in the circumferential direction. The ratio of areas under the orientation indicator (OI) curve in the range of $\pm10°$ from circumferential compared to $\pm10°$ from longitudinal was 2.7 for IEFs, 3.9 for SMC nuclei, and 2.2 for collagen fiber bundles. These circumferentially dominant ratios suggest that more than twice as many IEFs and collagen fibers and nearly 4 times as many SMC nuclei are aligned in the circumferential direction. We also noted that collagen fibers aligned preferentially in the media, but showed random orientation in the adventitia, with the media having a 60% greater ratio of area under the OI curve in the range of $\pm10°$ from circumferential compared to $\pm10°$ from longitudinal.

Discussion

In 1985, Clark and Glagov provided a 3D visual rendition of the architecture of the blood vessel mura, which has become the predominant image for understanding and modeling medial aortic structure. This fundamental MLU image has provided the foundation for understanding and

modeling of medial aortic structure. Evidence of a direct connection between IEFs and SMCs by Dingemans suggested a functional relationship between constituents.

This is the first time SBFSEM has been applied to the aorta. SBFSEM produces high resolution images of aortic medial microstructure that reveal the 3D architecture of all constituents. By imaging specimens in their physiological state, and removing constituents via image processing rather than chemical degradation, we show the true *in vivo* organization of mural constituents in both isolated and assembled configurations. The basic macro-structure of the MLU resembles Clark and Glagov's depiction. However, CLSM images resolve micro-scale features, such as the dense IEF network, staggered arrangement of elliptical SMC nuclei, and distribution of constituent orientation. SBFSEM images substantiate CLSM findings, and reveal new knowledge about nano-scale features such as shape and position of radial elastin struts, indentation and fibrous support structure of lamellar pores, complexity of IEFs, and spatial relationship among constituents. These novel features enhance our understanding of MLU microstructure (depicted in Figure 8).

General Medial Structure

MLU thickness measured using SBFSEM in our study agreed well with the 13-15μm previously reported using light and electron microscopy (Avolio et al., 1998; Clark and Glagov, 1985; Dingemans et al., 2000; Rodin, 1980; Wolinsky and Glagov, 1964; Wolinsky and Glagov, 1967). SBFSEM measurements of elastic lamellar thickness were comparable with previous studies showing 1.0-2.2 mμ (Dingemans et al., 2000; Sato et al., 1994). Previous research has shown asymmetry of aortic lamellae (Draney, 2003). Our results showed that even the rat, averaging only 4 lamellae has significant asymmetry in number of lamellae around the vessel circumference. Possible explanations for structural asymmetry of lamellae is greater anterior vessel strain (Draney, 2003) and lack of external support. Previous reports have shown lamellar branching (Berry, 1976; Gerrity, 1972; Smith, 1976), but our CLSM study showed that branching occurs regularly throughout the vessel circumference. This branching of lamellae provides an explanation of how this change in number of lamellae is structurally accommodated, and provides a means for local structure to match local strains without structural discontinuity.

All 3 primary vessel constituents showed preferential orientation in the circumferential direction. Mechanical vessel properties reflect this same circumferential dominance. Circumferential-to-longitudinal stress ratio is ~1.5,(Doyle and Dobrin, 1971; Vaishnav et al., 1972) and circumferential-to-longitudinal stretch ratio is 1.8 in the physiological regime (Shadwick and Gosline, 1994). The ratio of circumferential-to-longitudinal yield strength is 1.4.(Mohan and Melvin, 1982; Thubrikar et al., 2001) This preferential orientation of medial constituents in the same direction as the dominating physiological load and vessel mechanical properties suggests a strong relationship between vessel microstructure and function.

Elastin

Our volume measurement of elastin from SBFSEM images compared favorably with those reported previously (23%(He and Roach, 1994), 28%(Song and Roach, 1984)). A surprisingly large amount of elastin (nearly 1/3rd of all elastin) was not in the form of lamellae, but rather took the form of IEFs. Preferential circumferential orientation of IEFs suggests that elastin contributes to vessel anisotropy, predominantly in the physiological range, as previously reported by Sherebrin (Sherebrin et al., 1983). The observed abutment of IEFs to SMC cytoplasm confirmed the direct connection described by Dingemans (Dingemans et al., 2000). Through these connections, IEFs have a means of transferring lamellar stress to SMCs, the single living constituent within the aortic wall.

Radial elastin struts have been observed in TEM and SEM images of chemically degraded specimens (Berry, 1976; Smith, 1976; Song SH, 1985). The presented SBFSEM volume revealed the undisturbed configuration of thick radial elastin struts spanning the interlamellar space, and showed how struts provide radial connection of lamellae and division between SMCs. Struts comprised only a small fraction of elastin volume, but their sizeable thickness and dominant radial orientation suggested that they may play a key role in supporting radial loads within the elastin matrix, serving to prevent aortic dissection or delamination. Lamellar pore openings also showed radial support on the abluminal side by an extensive IEF network, likely reducing excessive deformation or displacement of pore edges.

Smooth Muscle Cells

Our measured SBFSEM volume of SMCs agreed well with previous studies of 23% (He and Roach, 1994), with relatively consistent proportions of cytoplasm and nuclei. The elliptical shape of SMC nuclei suggests that cells exist in tension, elongated by IEFs from adjacent lamellae. Matsumoto showed that radially cut aortic segments reveal protruding elastic lamellae and retracted SMCs, indicating that medial elastin exists in a state of compression and SMCs in a state of tension (Matsumoto T, 2003). That the SMC is oriented in the same preferential circumferential orientation as the other ECM constituents suggests that SMCs may be actively involved in mural support.

Previous studies have described an oblique orientation of SMCs, with only Fujiwara measuring the angle of tilt (Davis, 1993; Dingemans et al., 2000; Fujiwara and Uehara, 1992). Fujiwara reports an average of 23° for the rat thoracic aorta (Fujiwara and Uehara, 1992). We report a slightly lower value of 19° for the rat abdominal aorta. This radial tilt of SMC nuclei has typically been described as a herringbone arrangement, with SMC tilt alternating between layers (Davis, 1993; Dingemans et al., 2000). However, our study showed that the radial tilt of SMCs remained consistent between lamellae (Figure 8).

Individual SMCs were found between and around numerous IEFs, similar to the "musculo-elastic fascicles" described by Clark (Clark and Glagov, 1985). The similarity in orientation of IEFs and SMCs and the close proximity of termination points support Dingemans' report of a direct IEF to SMC cytoplasm connection. (Dingemans et al., 2000) Elastin forms cage-like structures around SMCs, with lamellae covering luminal and adventitial surfaces, and radial struts and IEFs dividing adjacent SMCs in the axial direction. SMCs freely connect to SMCs in the circumferential direction.

The elongation of the inner nucleus within a more flexible cytoplasm suggests that forces applied to the cytoplasm surface are transferred to the nucleus. Ingber showed that the SMC cytoplasm is filled with a cytoskeletal matrix that transmits forces from outside of the cell into the nucleus (Ingber, 2006; Ingber et al., 1994). In this manner, pulsatile cyclic stresses on the cell surface can influence gene transcription (Chiquet, 1999; Ingber, 2006). SMCs are responsible for synthesizing ECM to support the vessel wall. Cyclic tensile stress promotes the SMC to take on a contractile phenotype, decrease matrix metalloprotease (MMP) production, and generate moderate amounts of ECM (Chiquet, 1999; Kanda and Matsuda, 1994; Kim and Mooney, 2000). Conversely, zero stress causes SMC apoptosis, and static stress causes a synthetic SMC phenotype with increased MMP production and ECM synthesis (Kanda and Matsuda, 1994; Kim and Mooney, 2000). These previous studies show that SMC stimulus is linked to maintenance of mural function. Our study shows that the architecture of IEFs is one means by which physical stimuli might be transmitted.

Collagen

Collagen is commonly described and modeled as a meshwork of helically woven fibers layered around the vessel circumference (Clark and Glagov, 1985; Walker-Caprioglio et al., 1991). However, CLSM images showed that collagen fiber bundles were not woven together. Rather, fiber bundles were parallel within each layer. If the full stack of many parallel fiber layers was viewed through the entire thickness, it creates the appearance of a woven helical mesh arrangement. It is possible that this full thickness view caused this misinterpretation of collagen arrangement. Parallel fiber bundles suggest greater packing efficiency, allowing more fibers to be located in a smaller volume. Collagen fibers are oriented parallel in the highest loaded physiological structures (tendons and ligaments), suggesting that this parallel arrangement is favorable for high loading conditions. Our results show that collagen fibers are arranged to support loads preferentially in the circumferential direction.

Previous studies suggest that only 6-7% of collagen fibers are engaged at physiological pressure (Armentano et al., 1991; Greenwald et al., 1997). Our study visually confirmed that collagen fiber bundles were not taut at mean physiological pressure, and estimated a comparable recruitment of collagen fibers.

IEFs and SMCs exhibited similar oblique (circumferential and radial) tilt, but large collagen fiber bundles lacked radial tilt. This confirms Dingemans' finding that collagen bundles are independent of elastin and SMCs, lacking direct connection and receiving loads based on the overall MLU state (Dingemans et al., 2000).

This detailed 3D view of the aortic media confirms and clarifies basic features of MLU organization: lamellar elastin structure, elastin fibrils protruding from lamellae, oblique SMCs, SMC cytoplasm connects to IEFs, helical collagen fiber bundles. It highlights several new features: complexity and density of IEFs, thick elastin struts, gusseted pores, extensiveness of SMCs, and layers of unidirectional collagen bundles. This work resolves previously contradictory findings by showing that SMC obliquity is consistent from layer to layer, and collagen is arranged as layers of parallel fiber bundles, rather than as layers of woven mesh.

In conclusion, the 3D microstructure of elastin is more extensive and complex than previously thought. Elastin is prominent throughout interlamellar space in the form of circumferential IEFs and radial elastin struts. Elastin's impressive fibrous support structure suggests that, in addition to damping and load carrying, elastin transmits tension, resists dissection, and provides the structural foundation for the ongoing remodeling of the aortic wall. The extensiveness of SMC cytoplasm and the elliptical orientation of nuclei suggest that SMCs undergo continuous cyclic loading and are actively involved in remodeling of the aortic media. Collagen fiber bundles are assembled as stacks of parallel layers. The microstructural organization of these primary constituents corresponds with the predominant stress imposed on and the mechanical properties exhibited by the vessel.

This new image of the MLU provides the first high resolution 3D image of the aortic media. The complex, interrelated architecture of constituents provides insight into the structure-function relationship of the aorta. The aorta is a composite material, whose constituents, architecture, and interconnections are vitally important to overall material performance. Given the critical role of elastin, we can appreciate how diseases such as aneurysm, Marfan's Syndrome, and Ehler's Danos alter mural structure and function. For example, Marfan's patients are more susceptible to aortic dissection. It would be interesting to determine if the radial support of struts and gusseted pores are decreased or absent in the aortic media of Marfan's patients. We can determine the effects of hypertension which increases MLU thickness but not MLU quantity. We can understand how MLU structure changes with the natural degradation of elastin that comes about with aging. Attempts to engineer artificial blood

vessels can be specifically targeted to emulate critical functions observed in the healthy MLU. As we learn how the healthy aorta becomes unhealthy, we can begin to effectively maintain wall structure, prevent mural degradation, and repair (or even replace) existing damaged tissue.

Experimental Procedures

Experiments were performed on 8 adult male Sprague Dawley rats of 300-400g. All animals were treated in compliance with local IACUC approval in accordance with ethical guidelines. The micro- and nano-structure of the abdominal aorta was measured by confocal microscopy for seven aortas and electron microscopy for one aorta.

Animals were anesthetized and the infrarenal aorta was exposed. After ligating branching vessels, a 2-3cm segment of the infrarenal aorta was harvested and prepared for microstructural analysis. All 8 cylindrical specimens were fixed at mean intraluminal pressure of 110mmHg using 4% paraformaldehyde. All images were performed on fixed specimens in vitro. Figure 1 shows the location of samples and scale of images taken with confocal microscopy and electron microscopy. Eight cross section images were taken around the circumference of the vessel at 45°increments. The anterior region of samples was imaged for en face CLSM and SBFSEM specimens.

Confocal Laser Scanning Microscopy (CLSM) Imaging

Confocal imaging was performed at the CSIF Facility in the Beckman Center at Stanford University Medical Center. Scanning was performed on a Zeiss LSM 510 Confocal Laser Scanning Microscope using single photon excitation with a 25mW Argon laser of 488nm and 514nm using oil immersion lenses. Elastin and collagen naturally autofluoresce, with slight overlap in excitation and emission wavelengths. We uniquely identified optimal imaging regions for elastin and collagen by analyzing excitation and emission spectra for digested normal rat abdominal aorta specimens. We found that isolated elastin excites maximally at 488nm (20% laser power) and emits in the region 500-550nm (band pass filter). Isolated collagen excites at 514nm (30% laser power) with emission and reflection optimal in the region of 500-530nm (band pass filter). Propidium iodide (PI) was used to stain cell nuclei, allowing nuclei to be excited with the same 514nm wavelength as collagen, while emissions was recorded above 615nm (low pass filter), easily distinguished from collagen. PI indiscriminately stains all nuclei, making it possible that any cell type (SMCs, fibroblasts, macrophages, …) was imaged. However, SMCs are the only cell type observed in the healthy aortic media.(Ross and Glomset, 1973)

En face specimens were prepared by longitudinally slicing open the posterior side of the cylindrical specimen and laying it flat between microscope slide and coverslip. _En face_ images were recorded at 100× with slices taken at 0.37μm depth to give a voxel size of 0.09μm × 0.09μm × 0.37μm and field of view of 92μm × 92μm. Cross sections of 20-40μm thickness were imaged at 63× magnification to give a field of view (FOV) of 150μm × 150μm.

Serial Block Face Scanning Electron Microscopy (SBFSEM) Imaging

Approximately 1mm^2 pieces from the anterior wall of a single pressure-perfusion fixed specimen were soaked in 4% tannic acid with 2% gluteraldehyde and sodium cacodylate buffer at pH 4.0-4.3 for 12 hours to increase intensity of elastin in electron microscopy (EM) images. The specimen was rinsed in sodium cacodylate buffer and routinely processed for transmission electron microscopy (TEM) study using osmium post-fixation and uranyl acetate en bloc staining. Final embedding used hard formulation epoxy resin (Embed 812) to optimize thin sectioning. Following standard thick and thin section study, the specimen was mounted on

aluminum pins and trimmed to a cutting face of approximately 250×350μm, specific to the cutting apparatus of the SBFSEM machine.

Image stacks were then obtained using SBFSEM (Denk and Horstmann, 2004). The equipment consists of a scanning electron microscope (SEM) retrofitted with an in-chamber custom-built ultramicrotome that repeatedly removes uniform 40nm sections from the specimen surface, thereby exposing subsequent surfaces for block-face imaging by the SEM. Because the tissue block position is fixed, image registration is inherent and image distortion (as in TEM) is absent, greatly simplifying volume reconstruction.

Magnification of 5000× provided 2048×1768 pixels encompassing a 52×45 mμ^2 area of tissue. 1300 two-dimensional (2D) slices (5 GB of data) at 40nm thickness were used for volume rendering to generate the 3D images presented (25nm $\times$ 25nm $\times$ 40nm voxels). Separation of constituents (elastin, SMC nuclei, SMC cytoplasm, and collagen) required both automatic and manual segmentation. Manual segmentation of SMC nuclei and cytoplasm was performed on odd slices for a single SMC, and on every 8 slices for all SMCs within a single MLU. Pixels specific to each constituent were mapped into one of four gray-scale ranges. Using these gray-scale ranges, we assigned voxels for each constituent a specific range of color for viewing, and measured volume of voxel groups.

Quantification of Properties

Vessel diameter and mural thickness were measured from cross sections viewed under a light microscope. Medial thickness was measured as the distance from the internal elastic lamina to the outermost lamina. Lamellar number was estimated from the average of eight 2D CLSM cross sectional images taken at 45° increments around the vessel circumference. MLU quantity is computed as one less than the average quantity of lamellae, and MLU thickness is computed as medial thickness divided by MLU quantity.

Constituent Volumes

Volumes of elastin, SMC cytoplasm, SMC nuclei, and collagen were measured in SBFSEM volumes using the GE Advantage 4.3 system in Stanford University's 3D Imaging Lab. Volumes are reported as percent of total tissue volume. By using image processing to selectively measure constituent volumes in the tissue's _in vivo_ state, finer structures are preserved down to the resolution of the SBFSEM voxel (25nm $\times$ 25nm $\times$ 40nm).

The specific volumes of elastic features were measured in SBFSEM images. Lamellae volume was estimated based on lamellar dimensions in the SBFSEM volume. Radial elastin strut thickness and density were manually measured in 9 struts observed. Strut volume was estimated based on columnar strut shape and density. IEF volume was computed as total elastin volume minus lamellae and strut volume.

Nuclei volume was computed for all cells in the SBFSEM sample (N=39), and cytoplasm was computed for each cell contained between the two most prominent lamellae (N=10). Ellipticity of nuclei was measured by orienting the 3D volume to view maximal cell length, and computing ellipticity as nuclei long axis/ short axis. Radial tilt of SMC nuclei was computed with the SBFSEM volume oriented to view maximal nucleus length, using adjacent lamellae as the reference frame. As seen in Figure 1, lamellae were essentially parallel to each other and the lumen surface. Thus, the resulting radial tilt was defined parallel to the lumen surface. The

angle of radial tilt was computed as: $\text{RadicalTilt} = \sin^{-1}\left(\frac{L_N}{L_L}\right)$, where L_N is the length of the projected nucleus long axis, and L_L is the perpendicular distance between lamellae. Density of medial cell nuclei was quantified by counting cell nuclei within the media of both CLSM

and SBFSEM 3D volume images. Surface area-to-volume ratios were obtained from SBFSEM images using MATLAB (The Mathworks, Natick, MA). SMC perimeter and area were converted into surface area and volume, respectively, using the standard 40nm thickness of each 2D slice.

Number of fibers in collagen bundles was measured directly from 2D SBFSEM images. Averages were computed from over 100 measurements.

Fiber Orientation

Orientation of IEFs, collagen fibers, and cell nuclei were quantified using an orientation indicator (OI) based on two-dimensional discrete Fourier transforms (DFT) performed on _en face_ CLSM slices. The DFT was computed for each slice, and its magnitude was weighted to emphasize structures in the image with a specified spatial periodicity (corresponding to elastin and collagen structures repeating every 1.5-2.3μm and SMC nuclei repeating every 1-9μm). The central value of the projection of each weighted DFT was then computed for all projection angles using the radon transform as computed in MATLAB. The OI at each angle was computed by averaging these central values for a set of CLSM slices and normalizing these values to a mean of one. High values of OI at 90° correspond to circumferential orientation of structures with the specified spatial periodicity, whereas high values of OI at 0° and 180° correspond to longitudinal orientation. Windowing was performed on each image using Tukey windows to remove spurious peaks of the OI at 0°, 90°, and 180°. Medial and adventitial OIs were computed by using _en face_ slices corresponding to medial and adventitial regions, respectively. The ratio of areas under the OI curve in the range of ±10° from circumferential versus longitudinal was computed using OI values from 80° to 100°, divided by OI values from 0° to 10° and 170° to 180°.

Statistical values reported are based on a student's 2-tailed t-Test using 2-sample equal variance.

Acknowledgements

References

Armentano RL, Levenson J, Barra JG, Fischer EI, Breitbart GJ, Pichel RH, Simon A. Assessment of elastin and collagen contribution to aortic elasticity in conscious dogs. Am J Physiol 1991;260:H1870–1877. [PubMed: 1905490]

Arner A, Uvelius B. Force-velocity characteristics and active tension in relation to content and orientation of smooth muscle cells in aortas from normotensive and spontaneous hypertensive rats. Circ Res 1982;50:812–821. [PubMed: 7083482]

Avolio A, Jones D, Tafazzoli-Shadpour M. Quantification of alterations in structure and function of elastin in the arterial media. Hypertension 1998;32:170–175. [PubMed: 9674656]

Berry CL, Looker T, Germain J. The growth and development of the rat aorta. I Morphological aspects. J Anat 1972;113(Part1):1–16. [PubMed: 4648481]

Bierring F, Kobayasi T. Electron microscopy of the normal rabbit aorta. Acta Pathol Microbiol Scand 1963;57:154–168. [PubMed: 13968203]

Briggman KL, Denk W. Towards neural circuit reconstruction with volume electron microscopy techniques. Curr Opin Neurobiol 2006;16:562–570. [PubMed: 16962767]

Chiquet M. Regulation of extracellular matrix gene expression by mechanical stress. Matrix Biol 1999;18:417–426. [PubMed: 10601729]

Clark JM, Glagov S. Transmural organization of the arterial media. The lamellar unit revisited. Arteriosclerosis 1985;5:19–34. [PubMed: 3966906]

Cliff WJ. The aortic tunica media in growing rats studied with the electron microscope. Lab Invest 1967;17:599–615. [PubMed: 6074496]

Cliff WJ. The aortic tunica media in aging rats. Exp Mol Pathol 1970;13:172–189. [PubMed: 5470811]

Davis EC. Smooth muscle cell to elastic lamina connections in developing mouse aorta. Role in aortic medial organization. Lab Invest 1993;68:89–99. [PubMed: 8423679]

Denk W, Horstmann H. Serial block-face scanning electron microscopy to reconstruct three-dimensional tissue nanostructure. PLoS Biol 2004;2:e329. [PubMed: 15514700]

Dingemans KP, Teeling P, Lagendijk JH, Becker AE. Extracellular matrix of the human aortic media: an ultrastructural histochemical and immunohistochemical study of the adult aortic media. Anat Rec 2000;258:1–14. [PubMed: 10603443]

Dobrin, PB. Vascular Mechanics. Williams & Wilkins; Baltimore: 1983.

Doyle JM, Dobrin PB. Finite deformation analysis of the relaxed and contracted dog carotid artery. Microvasc Res 1971;3:400–415. [PubMed: 5130333]

Draney, M.; Xu, C.; Zarins, CK.; Taylor, CA. Circumferentially nonuniform wall thickness and lamellar structure correlates with cyclic strain in the porcine descending thoracic aorta. Paper presented at: ASME Summer Bioneginering Meeting; (Key Biscane, FL). 2003.

Driessen NJ, Peters GW, Huyghe JM, Bouten CV, Baaijens FP. Remodelling of continuously distributed collagen fibres in soft connective tissues. J Biomech 2003;36:1151–1158. [PubMed: 12831741]

Fujiwara T, Uehara Y. The cytoarchitecture of the medial layer in rat thoracic aorta: a scanning electron-microscopic study. Cell Tissue Res 1992;270:165–172. [PubMed: 1423519]

Gaballa MA, Jacob CT, Raya TE, Liu J, Simon B, Goldman S. Large artery remodeling during aging: biaxial passive and active stiffness. Hypertension 1998;32:437–443. [PubMed: 9740608]

Gabella, G. An introduction to the structural variety of smooth muscles. In: B., J., et al., editors. Vascular neuroeffector mechanisms: 4th International Symposium. Raven Press; New York: 1983. p. 13-35.

Gerrity RG, Cliff WJ. The aortuc tunica in young and aging rats. Exp Mol Pathol 1972;16(3):382–402. [PubMed: 4337757]

Gosline JM, Shadwick RE. The mechanical properties of fin whale arteries are explained by novel connective tissue designs. J Exp Biol 1996;199(Pt 4):985–997. [PubMed: 8788091]

Greenwald SE, Moore JE Jr. Rachev A, Kane TP, Meister JJ. Experimental investigation of the distribution of residual strains in the artery wall. J Biomech Eng 1997;119:438–444. [PubMed: 9407283]

Hansen TR, Dineen DX, Pullen GL. Orientation of arterial smooth muscle and strength of contraction of aortic strips from DOCA-hypertensive rats. Blood Vessels 1980;17:302–311. [PubMed: 7437523]

He CM, Roach MR. The composition and mechanical properties of abdominal aortic aneurysms. J Vasc Surg 1994;20:6–13. [PubMed: 8028090]

Ingber DE. Cellular mechanotransduction: putting all the pieces together again. Faseb J 2006;20:811–827. [PubMed: 16675838]

Ingber DE, Dike L, Hansen L, Karp S, Liley H, Maniotis A, McNamee H, Mooney D, Plopper G, Sims J, et al. Cellular tensegrity: exploring how mechanical changes in the cytoskeleton regulate cell growth, migration, and tissue pattern during morphogenesis. Int Rev Cytol 1994;150:173–224. [PubMed: 8169080]

Jackson ZS, Gotlieb AI, Langille BL. Wall tissue remodeling regulates longitudinal tension in arteries. Circ Res 2002;90:918–925. [PubMed: 11988494]

Jiang, CF,AA. Study of age-related changes in the elastic matrix of the human aorta using selective tissue digestion and scanning electron microscopy. Paper presented at: Proceedings of the 1992 International Symposium on Biomedical Engineering in the 21st Century; Taipai, Taiwan: HUEI-WEN Science Publishing Co; 1992.

Kanda K, Matsuda T. Mechanical stress-induced orientation and ultrastructural change of smooth muscle cells cultured in three-dimensional collagen lattices. Cell Transplant 1994;3:481–492. [PubMed: 7881760]

Keech MK. Electron microscope study of the normal rat aorta. J Biophys Biochem Cytol 1960;7:533–538. [PubMed: 14405104]

Kim BS, Mooney DJ. Scaffolds for engineering smooth muscle under cyclic mechanical strain conditions. J Biomech Eng 2000;122:210–215. [PubMed: 10923287]

Loree HM, Kamm RD, Stringfellow RG, Lee RT. Effects of fibrous cap thickness on peak circumferential stress in model atherosclerotic vessels. Circ Res 1992;71:850–858. [PubMed: 1516158]

Matsumoto, T.; G., T.; Sato, M. Residual stress and strain in the artery wall: from macroscopic to microscopic viewpoint. Proceedings of Advanced Technology in Experimental Mechanics; 2003. 0s07w0160

Mohan D, Melvin JW. Failure properties of passive human aortic tissue. I- -uniaxial tension tests. J Biomech 1982;15:887–902. [PubMed: 7161291]

Osborne-Pellegrin MJ. Some ultrastructural characteristics of the renal artery and abdominal aorta in the rat. J Anat 1978;125:641–652. [PubMed: 640965]

Pease DC, Paule WJ. Electron microscopy of elastic arteries; the thoracic aorta of the rat. J Ultrastruct Res 1960;3:469–483. [PubMed: 14431272]

Rhodin, J. Architecture of the vessel wall. In: Berne, R., editor. Handbook of Physiology. American Physiological Society; 1979.

Rodin, J. Handbook of Physiology. American Physiological Society; Bethesda: 1980. The architecture of the vessel wall; p. 1-31.

Ross R, Glomset JA. Atherosclerosis and the arterial smooth muscle cell: Proliferation of smooth muscle is a key event in the genesis of the lesions of atherosclerosis. Science 1973;180:1332–1339. [PubMed: 4350926]

Sato F, Shimada T, Kitamura H, Campbell GR, Ogata J. Changes in morphology of elastin fibers during development of the tunica intima of monkey aorta. Heart Vessels 1994;9:140–147. [PubMed: 8056720]

Shadwick RE. Mechanical design in arteries. J Exp Biol 1999;202:3305–3313. [PubMed: 10562513]

Sherebrin MH, Song SH, Roach MR. Mechanical anisotropy of purified elastin from the thoracic aorta of dog and sheep. Can J Physiol Pharmacol 1983;61:539–545. [PubMed: 6883206]

Smith P. A comparison of the orientation of elastic fibers in the elastic laminae of the pulmonary trunk and aorta of rabbits using the scanning electron microscope. Lab Invest 1976;35(6):525–529. [PubMed: 994464]

Song SH, Roach MR. Comparison of fenestrations in internal elastic laminae of canine thoracic and abdominal aortas. Blood Vessels 1984;21:90–97. [PubMed: 6696999]

Song SH, Roach MR. A morphological comparison of aortic elastin from five species as seen with the scanning electron microscope. Acta Anat 1985;123(1):45–50. [PubMed: 4050307]

Sun W, Sacks M, Fulchiero G, Lovekamp J, Vyavahare N, Scott M. Response of heterograft heart valve biomaterials to moderate cyclic loading. J Biomed Mater Res A 2004;69A:658–669. [PubMed: 15162408]

Thubrikar MJ, Labrosse M, Robicsek F, Al-Soudi J, Fowler B. Mechanical properties of abdominal aortic aneurysm wall. J Med Eng Technol 2001;25:133–142. [PubMed: 11601439]

Vaishnav RN, Young JT, Janicki JS, Patel DJ. Nonlinear anisotropic elastic properties of the canine aorta. Biophys J 1972;12:1008–1027. [PubMed: 5044576]

Walker-Caprioglio HM, Trotter JA, Mercure J, Little SA, McGuffee LJ. Organization of rat mesenteric artery after removal of cells of extracellular matrix components. Cell Tissue Res 1991;264:63–77. [PubMed: 2054846]

Wolinsky H, Glagov S. Structural Basis for the Static Mechanical Properties of the Aortic Media. Circ Res 1964;14:400–413. [PubMed: 14156860]

Wolinsky H, Glagov S. A lamellar unit of aortic medial structure and function in mammals. Circ Res 1967;20:99–111. [PubMed: 4959753]

Zatina MA, Zarins CK, Gewertz BL, Glagov S. Role of medial lamellar architecture in the pathogenesis of aortic aneurysms. J Vasc Surg 1984;1:442–448. [PubMed: 6481894]
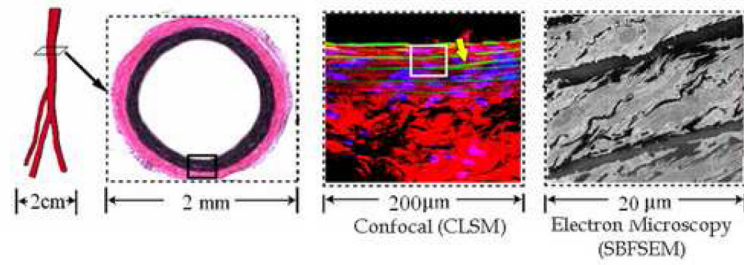
Figure 1. Sample Location and Size
Represents scale of imaging. Images presented are from (left to right) geometric model of rat aorta, light microscopy of aortic cross section, confocal laser scanning microscopy (CLSM), and serial block face scanning electron microscopy (SBFSEM). Note the branching lamellae in the CLSM image (yellow arrow).
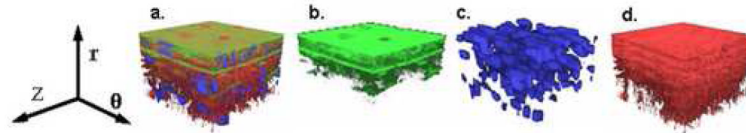
Figure 2. 3D CLSM Images Show *In Vivo* Arrangement of Combined and Individual Constituents
3D confocal images showing *in vivo* microstructure with green representing elastin, red collagen, and blue SMC nuclei. (a) Combined, (b) Elastin only, (c) SMC nuclei, and (d) Collagen only. Lumen surface located at top, circumferential direction noted. Volumes are 92μm × 92μm × 60μm. (r indicates radial direction, z axial, and θcircumferential).
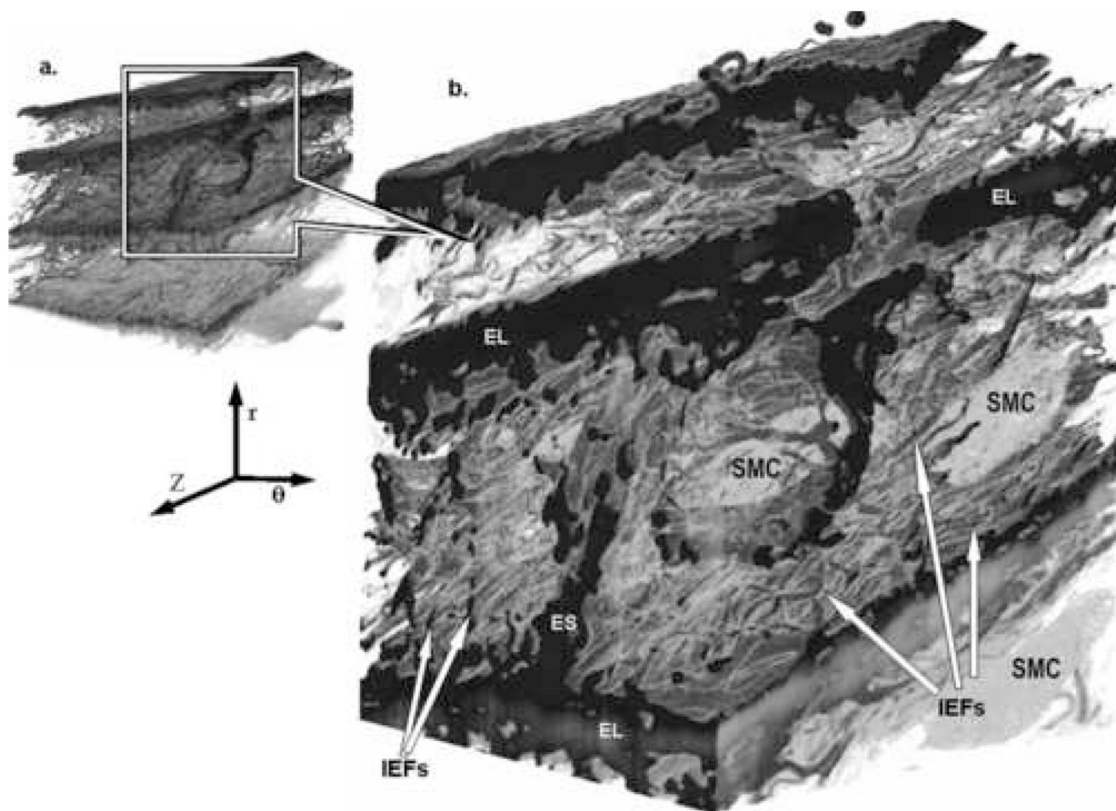
Figure 3. 3D SBFSEM Images Showing Elastin Features
SBFSEM images show how SMC nuclei (SMC) reside within the complex 3D architecture of elastin. (a. Full view, b. Magnified section). Thickness of elastic lamellae (EL) varies. 3 primary forms of elastin are evident, with continuous sheets of circumferential elastin forming elastic lamellae (EL), a dense network of interlamellar elastin fibers (IEFSs) protruding from top & bottom lamellar surfaces in oblique (circumferential & radial) directions, and a thick radial elastin strut (ES) connecting adjacent lamellae. (Small volume dimensions ($\theta \times Z \times r$) are $31\mu m \times 36\mu m \times 50\mu m$, and magnified volume $22\mu m \times 16\mu m \times 25\mu m$. (r indicates radial direction, z axial, and θ circumferential).
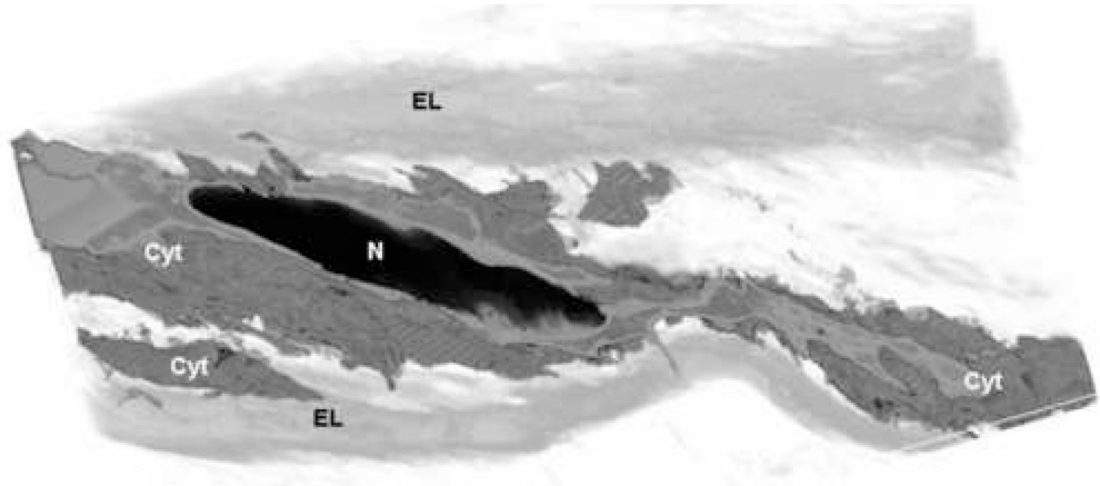
Figure 4. 3D SBFSEM Volume Showing Smooth Muscle Cell Configuration
Nuclei align between lamellae in staggered arrangement. The shape of healthy aortic smooth muscle cell nuclei is elliptical (Long axis/ radius = 6.2±1.4). The nuclei's long axis is oriented circumferentially with a 19°radial tilt that directs ends toward top & bottom lamellae. The cytoplasm weaves throughout interlamellar space, extending numerous offshoots. (N = Nuclei, Cyt = Cytoplasm, EL = Elastic Lamella)
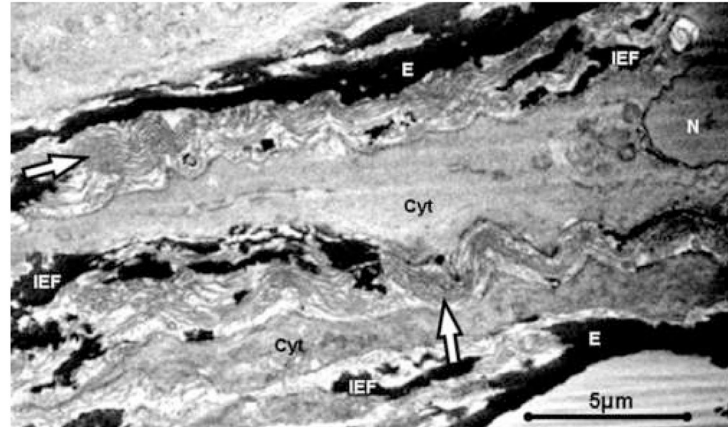
Figure 5. Sequential 2D CLSM Images Show Collagen Arrangement
Sequential confocal images of the media of one representative healthy rat abdominal aorta (Collagen = Red, SMC nuclei = Blue). The first image in the series is taken just below the internal elastic lamella, and each subsequent image is 2.2μm deeper. Collagen fiber bundles do not form a helical mesh within each layer, rather bundles are parallel within each layer, closely enveloping SMC nuclei. Fiber orientation for each layer differs slightly from adjacent layers, achieving a variation of orientations throughout mural thickness.
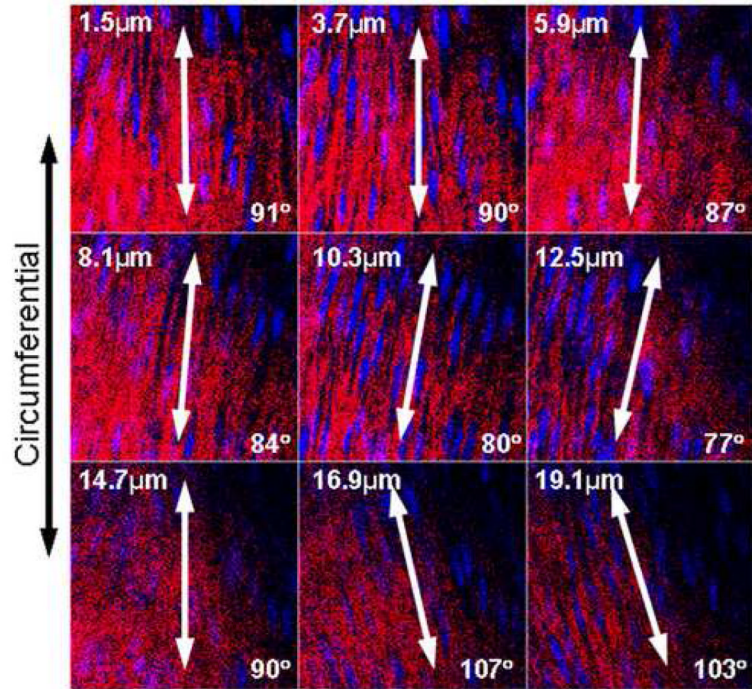
Figure 6. 2D SBFSEM Images Showing Helical Bundles of Collagen Fibers
2D SBFSEM image shows collagen fibers in bundles of 40-50 fibers (arrows). Collagen bundles do not appear taut, despite fixation of specimens at mean intraluminal pressure. Fiber bundles spiral in & out of image plane, suggesting helical rather than crimped structure. IEFs are seen extending circumferentially and radially throughout interlamellar space, with cytoplasm weaving in close proximity. (E = Elastic Lamella, IEF = Interlamellar Elastin Fiber, Arrow = Collagen fiber bundle, Cyt = SMC Cytoplasm, N = Nucleus).
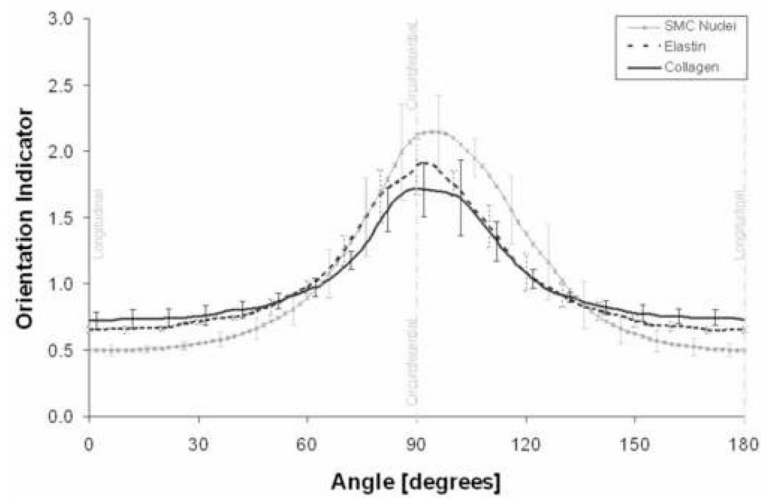
Figure 7. Distributed Orientation of Smooth Muscle Cell Nuclei, Elastin, & Collagen
Normalized distribution of orientation indicators (OIs) of mural constituents shows that smooth muscle cell nuclei, interlamellar elastin fibers, and collagen preferentially align in the circumferential direction (90°).
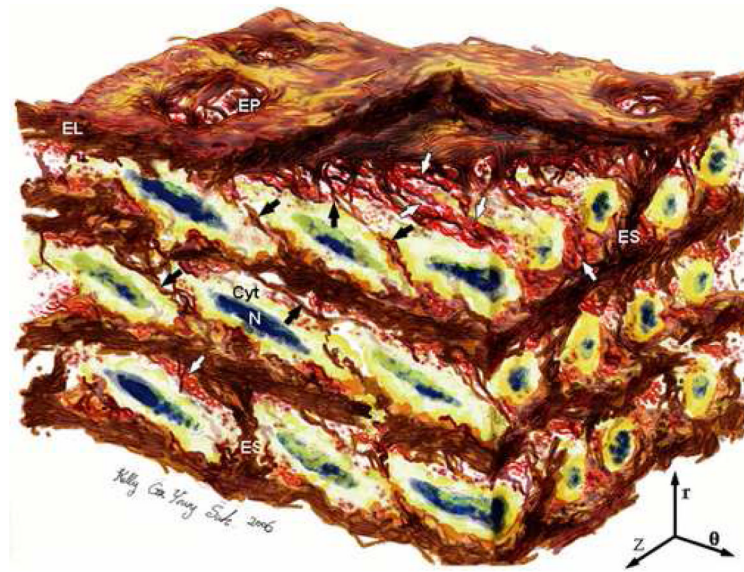
Figure 8. Revised 3D Medial Aortic Microstructure
Artistic rendering of aortic medial microstructure from SBFSEM volume. Aortic media shows complex, interconnected structure. **ELASTIN** features include elastic lamellae (EL), dense network of interlamellar elastin fibers (IEFs shown with black arrows), elastin struts (ES), & reinforced elastin pores (EP). **SMOOTH MUSCLE CELL** (SMC) features include staggered elliptical nuclei (N) oriented circumferentially with radial tilt, & cytoplasm (Cyt) abuts IEFs & overlaps adjacent SMCs. **COLLAGEN** features include large & small fiber bundles (white arrows) adjacent to lamellar surfaces, arranged in layers of parallel bundles oriented predominantly circumferentially. Image dimensions ($\theta \times Z \times r$) are 80μm × 60μm × 45μm, with lumen surface at top. (r indicates radial direction, z axial, and θcircumferential).

Table 1

Macroscopic Features & Composition of Healthy Rat Abdominal Aorta

Number of Medial Lamellae	4.4±0.5
Anterior	5.4±0.5[*]
Posterior	3.4±0.6[*]
Elastin Volume [%]	~29
Lamellae volume [%]	~71
IEF volume [%]	~27
Strut volume [%]	~2
Smooth Muscle Cell Volume [%]	~24
Nuclei Volume [%]	11 ±3
Cytoplasm Volume [%]	89 ±3
Ellipticity	6.2 ±1.4
Radial Tilt [degrees]	19.1 ±2.8
Collagen + Ground Substance Volume [%]	~47
Collagen Recruitment [%]	10 ±1

[*]
$p < 0.001$